Nanoscale

Accepted Manuscript

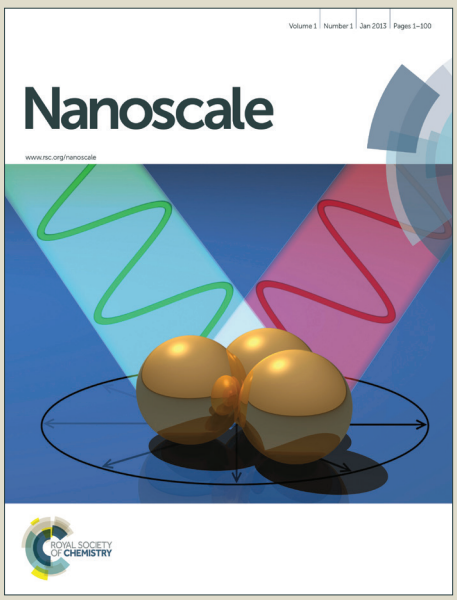

ROYAL SOCIETY OF CHEMISTRY

www.rsc.org/nanoscale

Graphene Nanosheets-Tailored PtPd Concave Nanocubes with Enhanced Electrocatalytic Activity and Durability for Methanol Oxidation

Yizhong Lu, [a,b] Yuanyuan Jiang [a,b] and Wei Chen *[a]

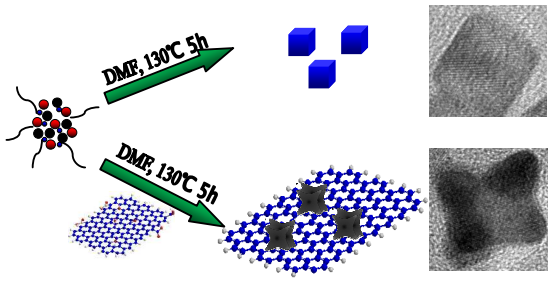

PtPd concave nanocubes could be tailored by graphene nanosheets and they exhibit enhanced electrocatalytic performance for methanol oxidation.

Cite this: DOI: 10.1039/c0xx00000x

www.rsc.org/xxxxxx

ARTICLE TYPE

Graphene Nanosheets-Tailored PtPd Concave Nanocubes with Enhanced Electrocatalytic Activity and Durability for Methanol Oxidation

Yizhong Lu,[a,b] Yuanyuan Jiang [a,b] and Wei Chen*[a]

Received (in XXX, XXX) Xth XXXXXXXXX 20XX, Accepted Xth XXXXXXXXX 20XX
DOI: 10.1039/b000000x

Here, we demonstrate that graphene oxide (GO) can act as a structure-directing agent for the formation of PtPd alloy concave nanocubes enclosed by high index facets. Under the presence of GO, PtPd alloy concave nanocubes could be easily tailored by a simple hydrothermal reaction. In sharp contrast, only cubic PtPd alloy nanocrystals were obtained with the absence of GO. Moreover, compared to the unsupported PtPd nanocubes, the composition ratio of Pt to Pd changed significantly from 1:1 to 3:1. Due to the exposed high-index facets and the strong interaction between catalysts and graphene support, the as-synthesized PtPd concave nanocubes exhibited enhanced electrocatalytic activity and highly durability toward methanol oxidation. The present work highlights the unique role of GO in the formation of metal nanocrystals as not only a catalyst support but also a structure- and/or morphology-directing agent, due to the presence of various functional groups on GO sheets. The present GO-assisted approach provides a new avenue to the synthesis of nanocrystals with high-index facets and initiates new opportunities for the exploration of high-performance graphene-based nanocatalysts.

1. Introduction

Nanostructured PtPd materials have attracted great interest due to their promising applications in electrocatalysts.[1-4] Generally, the catalytic performance of nanocrystals can be finely manipulated either by changing their compositions, which mediate the electronic structures, or by controlling their shapes**,** which determine the exposed surface atomic arrangement and coordination.[5-9] As a result, recent years have witnessed tremendous efforts devoted to the design, synthesis, and utilization of noble metal nanocrystals with a variety of compositions and shapes. Although various PtPd nanocrystals with different morphologies have been reported, most of the nanocrystals demonstrate convex shapes enclosed by low-index facets as a result of minimization of the surface energy. Interestingly, recent studies have shown that metal nanocrystals with high-index facets, which possess a high density of low-coordinated atoms, steps, edges, and kinks, exhibited much higher catalytic activity, selectivity, and stability as fuel cell electrocatalysts for the electrooxidation of small organic fuels and the oxygen reduction reaction.[10-13] Meanwhile, a number of different procedures have also been developed for the synthesis of noble-metal nanocrystals with concave surfaces. In general, two strategies (i) site-specific dissolution through etching and galvanic replacement, and (ii) directionally controlled overgrowth by facet-selective capping, kinetic control, and template-directed epitaxy were used to realize the production of concave nanocrystals.[13-16] However, the average size of the reported concave crystals is still rather large (20-240 nm) for their application as electrocatalysts, since nanocatalysts with size smaller than 20 nm are desirable.[17] Therefore, the synthesis of concave nanocrystals with reduced size remains challenging. Moreover, the reported syntheses suffer from the multiple steps.

On the other hand, catalyst support materials play a vital role in improving the catalytic activity and reducing the catalyst loading.[18, 19] Nowadays, the severe corrosion and oxidation of the carbon supports in the harsh operating environment would lead to the quick loss of the electrocatalytic activity of the supported catalysts.[20, 21] In recent years, graphene has attracted much attention for potential applications as unique 2D catalyst support due to its intrinsic material properties including low cost, high surface area, good electrical conductivity and high mechanical strength, which can not only maximize the availability of nanosized electrocatalyst surface area, but also provide enhanced mass transport.[22-24] As for graphene-metal hybrid catalysts, it was proposed that the strong coupling between graphene and catalyst play an important role in enhancing their catalytic activities.[23, 25, 26] Therefore, nanocatalysts directly grown on graphene sheet can efficiently maximize the graphene-catalyst contact and thus achieve the desired high catalytic activity and high durability. Unfortunately, *in situ* growth of metal nanocrystals on graphene currently lack effective control over the desired size, morphology, and structure, and as a result, their catalytic potentials may not be fully realized. Additionally, few studies have been focused on the role of graphene during the formation of metal nanocrystals.

Based on above facts, here, we demonstrate for the first time

the key role played by GO in the controlled synthesis of PtPd alloy concave nanocubes enclosed by high-index facets. Different from the previously reported electrochemical and wet chemical approaches, the present study provides a novel one-step synthetic strategy for the *in situ* synthesis of concave PtPd nanocubes on reduced GO nanosheets (C-PtPd/RGO). The catalytic properties of the C-PtPd/RGO were then evaluated by employing the oxidation of methanol as a model reaction. It was found that the as-synthesized C-PtPd/RGO display enhanced methanol oxidation activity with peak current density up to 381 mA mg^{-1}, which is nearly 3.66 times higher than that of the commercial Pt/C catalyst. In addition, the electrochemical active surface area (ECSA) showed only 9.96% loss after 1000 voltammetric cycles and almost no activity loss in the form of peak current density. The enhanced electrocatalytic activity and durability could be ascribed to the tailored concave structure with high-index facets and the strong interaction between the PtPd nanocrystlas and the RGO nanosheets support.

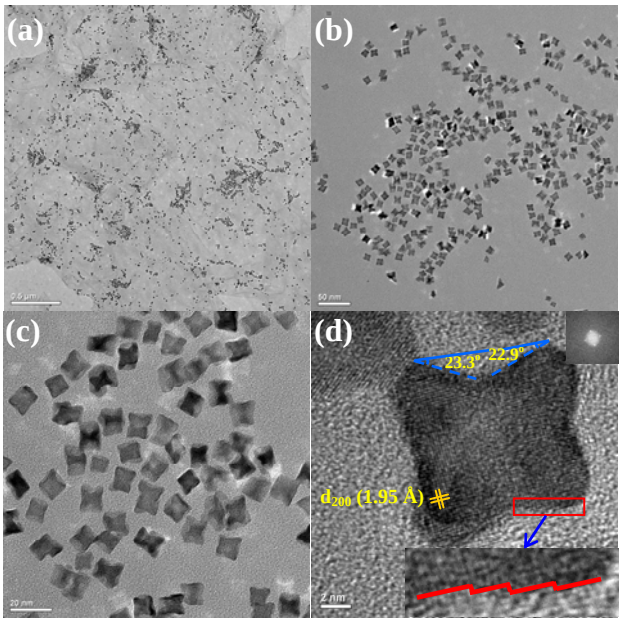

Fig. 1 (a, b) Representative TEM images of C-PtPd/RGO at different magnifications. (c, d) HRTEM images of the as-synthesized C-PtPd/RGO at different magnifications. The inset in the top right in e shows the FFT pattern of the concave nanocube and the inset in the bottom right is a zoom-in image of the selected area marked by red rectangle in d.

2. Results and Discussion

2.1 Synthesis and characterization of graphene nanosheets-tailored PtPd concave nanocubes

By using a facile hydrothermal synthetic strategy, RGO-supported PtPd alloy concave nanocubes (C-PtPd/RGO) were synthesized in the presence of GO. To prepare the C-PtPd/RGO, the mixture of K_2PtCl_4 and Na_2PdCl_4 with a molar ratio of 50:50, PVP, aqueous NaI solution, and DMF solution of GO was put in a Teflon-lined stainless steel autoclave and heated at 130 °C for 5 h. The C-PtPd/RGO was obtained after centrifugation and purification (see Experimental Section for details). Fig. 1a and b displays the TEM images of the as-prepared C-PtPd/RGO at different magnifications. It can be seen that almost all the produced nanocrystals exhibit cubic shape with concave structure (nearly 100 %) and are uniformly dispersed on RGO sheets. From the particle size distribution histogram shown in Fig. 3h, the as-prepared concave nanocrystals have an average size of 13.80 ± 0.05 nm. However, with the absence of GO during the hydrothermal process, uniform PtPd alloy nanocubes (Fig. S1) were produced. Note that the size of the PtPd alloy concave nanocubes supported on RGO is slightly larger than that of the unsupported PtPd alloy nanocubes (~ 12.0 nm). The different size and shape of the nanocrsytals indicate the key role of GO in determining the morphology of the PtPd products, where GO can influence the nucleate and/or growth process of the nanocrystals.

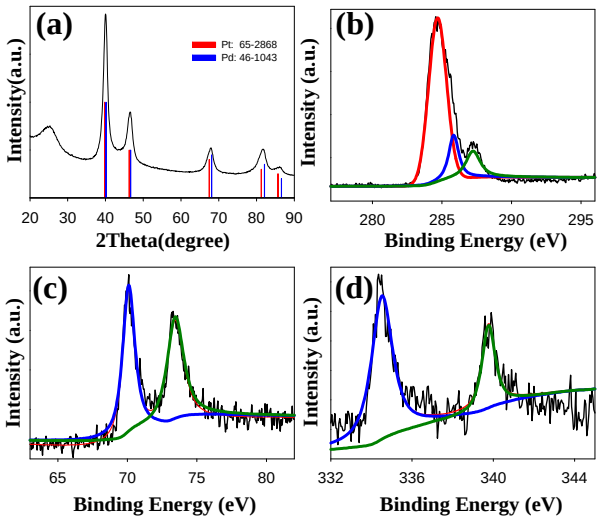

Fig. 2 (a) XRD pattern of the C-PtPd/RGO composites. For comparison, bulk Pt (red bars) and Pd (blue bars) from the JCPDS were also included. (b-d) XPS of C 1s, Pt 4f and Pd 3d, respectively.

HRTEM and EDX measurements were carried out to characterize the morphology, crystal structure, and composition of the C-PtPd/RGO. The HRTEM images (Fig. 1c, d) shows that all of the as-synthesized PtPd nanocrystals exhibit a distinct cubic shape with concave structure. For a concave nanocube enclosed by high-index facets, the Miller indices can be derived from the projection angles along a selected crystallographic axis.[15] A HRTEM image taken from an individual concave nanocube (Fig. 1d) viewed along <100> zone axis, as confirmed by the corresponding fast Fourier transform (FFT) pattern (Fig. 1d inset, top right), indicates that each nanocube is a single crystal with well-defined fringes. The interplanar distance of the lattice fringes was measured to be 0.195 nm, corresponding to the interplanar (200) distance of fcc Pt and Pd.[25, 27] The measured projection angles were calculated to be 22.9 and 23.3°. Based on the previous report, the high-index facets could be indexed as the {730} planes.[15] Moreover, the high-magnification HRTEM image clearly shows the presence of high-index steps (Fig. 1d inset, bottom right). The overall weight percentage of Pt in the cubic nanocrystals was further determined to be 73.5% and 75%, respectively, from energy-dispersive X-ray

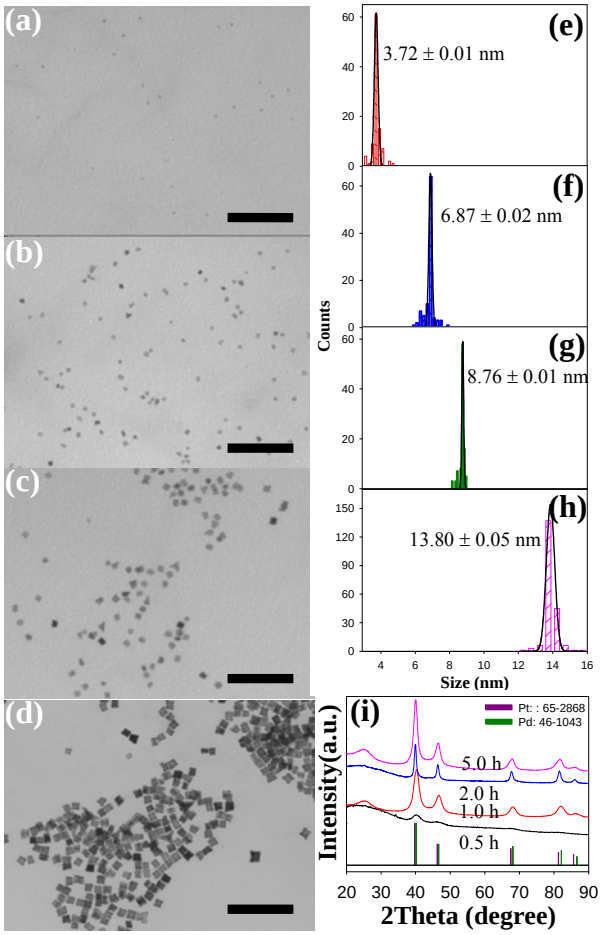

Fig. 3 Representative TEM images and the size distribution histograms of the products collected at different reaction time: (a, e) 0.5 h, (b, f) 1.0 h, (c, g) 2.0 h and (d, h) 5 h. Scale bars in all the TEM images are 100 nm. (i) XRD patterns of the products obtained at different reaction time.

spectroscopy (EDX, Fig. S2a) and inductively coupled plasma-atomic emission spectrometry (ICP-AES) analyses. Note that the weight percentage is much different from that of the unsupported PtPd alloy nanocubes synthesized without GO (Pt: Pd=51: 49, Fig. S2b), further indicating the influence of GO on the composition of PtPd nanocrystals.

In the XRD pattern of the C-PtPd/RGO composites (Fig. 2a), the diffraction peaks with 2θ centered at 40.0, 46.5, 67.8 and 81.7° could be indexed to the (111), (200), (220), and (311) planes of face-centered cubic (fcc) lattice structure. It should be noted that, the diffraction peaks from the C-PtPd/RGO locate between the positions from pure Pt (red bars) and Pd (blue bars), strongly indicating the formation of alloyed PtPd nanocrystals. The broad peak at 2θ ≈25° can be assigned to the (002) plane of the stacked RGO sheets.[28] These XRD results indicate that the formation of concave PtPd nanocrystals and the reduction of GO sheets to RGO occur simultaneously during the hydrothermal process. According to the Scherrer's equation, he average size of the PtPd concave nanocubes was also calculated to be approximately 14.0 nm based on the (200) peak, which is in good agreement with that from the TEM measurement. X-ray photoelectron spectroscopy (XPS) measurements were then performed to determine the chemical states and compositions of carbon, Pt, and Pd in the C-PtPd/RGO. The deconvoluted C 1s spectrum of GO is shown in Fig. 2b. Compared to the pristine GO,[29] the peak intensities of C-O and C=O in the C-PtPd/RGO decreased significantly, indicating that most oxy-functional groups have been removed after the hydrothermal process. Fig. 2c and d shows the Pt 4f and Pd 3d regions of the deconvoluted XPS spectrum of the C-PtPd/RGO. The peaks at 70.1 and 73.5 eV in the Pt 4f spectrum could be assigned to the binding energies of Pt $4f_{7/2}$ and Pt $4f_{5/2}$ of metallic Pt^0, respectively.[30] The peaks at 334.5 and 339.7 eV in the Pd XPS spectrum are attributed to the binding energies of Pd $3d_{5/2}$ and Pd $3d_{3/2}$, respectively. These binding energies are comparable to those of palladium metal, confirming the zerovalent state of the Pd.[31] In addition, similar to the EDX and ICP-AES results, the weight ratio of Pt/Pt was also determined to be 74 : 26 from the XPS analysis. These XPS data further indicate that Pt and Pd precursors and GO have been reduced simultaneously during the hydrothermal process.

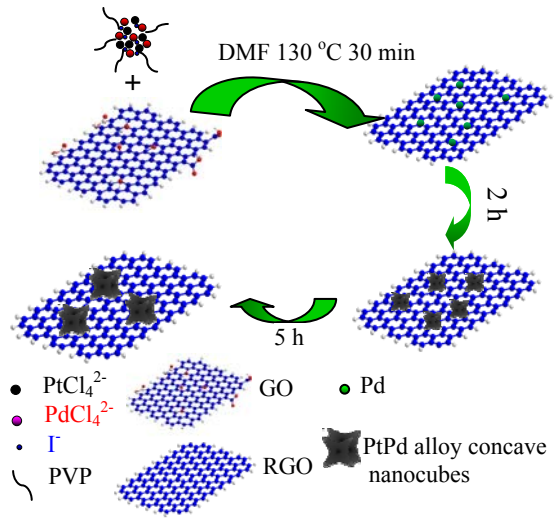

Scheme 1 Schematic illustration for the graphene nanosheets-tailored synthesis of RGO-supported PtPd alloy concave nanocubes (C-PtPd/RGO).

Overall, the presence of GO during the synthesis could not only influence the morphology (concave *vs* convex), but also play a key role in determining the composition (3:1 *vs* 1:1) of the PtPd alloy nanocrystals. To better understand the formation process of C-PtPd/RGO composites, aliquots at different reaction times were taken for TEM analysis. Fig. 3 shows the morphological evolution and size change of the nanocrystals with reaction time. It can be seen that after reaction for 30 min, only small nanoparticles with an average size of 3.72 nm were produced (Fig. 3a and e). With the reaction time increasing, the size of the nanoparticles continues to grow with the average size of 6.87 and 8.76 nm, respectively, after 1 (Fig. 3b and f) and 2 h (Fig. 3c and g). However, the concave structure could not be clearly observed until the reaction durations of 5 h with an average size of 13.80 nm (Fig. 3d and h), and no further growth and morphology change were observed even after prolonged heating for 8 h (Fig. S3). XRD and XPS analyses

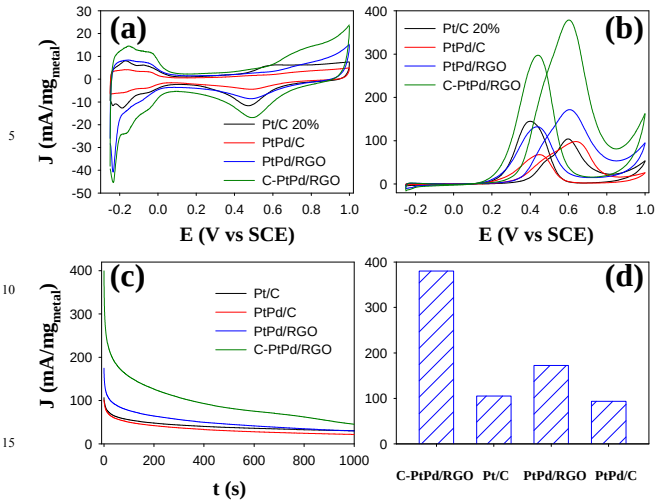

Fig. 4 CVs of the C-PtPd/RGO, commercial Pt/C, PtPd/RGO, and PtPd/C in (a) 0.5 M H_2SO_4 solution and (b) 0.5 M H_2SO_4 + 0.5 M CH_3OH solution. (c) Chronoamperometric curves of methanol oxidation at 0.60 V in 0.5 M H_2SO_4 + 0.5 M CH_3OH solution. Potential scan rate of 50 mV s^{-1}. All curves were normalized to the total mass of noble metals (Pt + Pd). (D) Comparison of the mass specific activity of the different electrocatalysts at 0.60 V.

were then performed to unravel the composition evolution of the C-PtPd/RGO composites. Fig. 3i shows the XRD patterns of the products obtained at different reaction stages. The diffraction peaks exhibit an obvious blue shift with reaction time. From the positions of the diffraction peaks, Pd nanoclusters were first formed and then Pt content began to increase with reaction time until the complete consumption of the metal precursors. XPS analysis indicated that the Pt content increased from 0 to 23, 51, and finally to 74%.

Based on the present and previously reported results,[25, 27] we propose a reasonable formation mechanism of the C-PtPd/RGO composites, as shown in Scheme 1. Firstly, GO was reduced to RGO when the temperature was raised to 130 °C, and simultaneously, Pd nanoclusters were formed and deposited on the RGO sheets due to their strong interaction. The galvanic replacement reaction between the as-synthesized Pd nanoclusters and Pt precursors then occurred, followed by the co-reduction of Pt and Pd precursors, finally resulting in the formation of RGO-supported concave alloy nanocrystals. From the formation of concave or cubic PtPd nanocrystals with or without the presence of RGO, RGO may influence the reaction kinetics of the nucleation and/or crystal growth and thus direct the formation of concave structure. Here, the controlled synthesis of concave structure in the presence of GO may be thus ascribed to the fast co-reduction rate of Pt and Pd precursors on the (111) facets and relatively low rate of galvanic placement on (100) surface due to the presence of I^-, which is selectively adsorbed on the (100) facets of Pd nanocrystals. More mechanism study is currently underway.

2.2 Electrocatalytic performance of graphene nanosheets-supported PtPd concave nanocubes (C-PtPd/RGO) for methanol oxidation

Due to the high-density of atomic steps and kinks on high-index surfaces, the C-PtPd/RGO composites are expected to have high electrocatalytic activity. The methanol oxidation reaction (MOR) catalyzed by the C-PtPd/RGO was then studied. For comparison, MOR on the commercial Pt/C catalyst (20% Pt loading with a particle diameter of about 3 nm), carbon supported PtPd alloy nanocubes (PtPd/C, 20% metal loading), and RGO supported PtPd alloy nanocubes (PtPd/RGO, 20% metal loading) were also measured. The TEM images of these catalysts are shown in Fig. S4. Before the electrochemical measurements, all the glassy carbon (GC)-supported catalysts were subjected to argon plasma treatment, electrochemical polishing between -0.25 and 1.0 V, and CO stripping to obtain surface-clean electrocatalysts. Fig. 4a shows the typical cyclic voltammetry (CV) curves recorded in nitrogen-saturated 0.5 M H_2SO_4 aqueous solution at a scanning rate of 50 mV s^{-1}, with the current density normalized to the loading of metal mass (Pt and Pd). Note that the double-layer capacitance of the RGO-supported PtPd catalysts is much larger than that of the carbon supported ones, indicating the large surface area of graphene nanosheets, which renders them suitable support for the good dispersion of nanoparticle catalysts. From the charge involved in the hydrogen adsorption/desorption, the electrochemically active surface area (ECSA) of the C-PtPd/RGO, Pt/C, PtPd/C, and PtPd/RGO were calculated to be 317, 157, 87.6, and 187cm^2 mg_{metal}^{-1}, respectively. It can be seen that the as-synthesized C-PtPd/RGO composites display the largest ECSA, which might be attributed to the unique concave morphology as well as well dispersion of PtPd catalysts on RGO surface. On the other hand, the ECSA of PtPd alloy nanocubes supported on RGO is much larger than that on carbon black. The CV measurements further suggest that RGO is a good candidate as catalyst support.

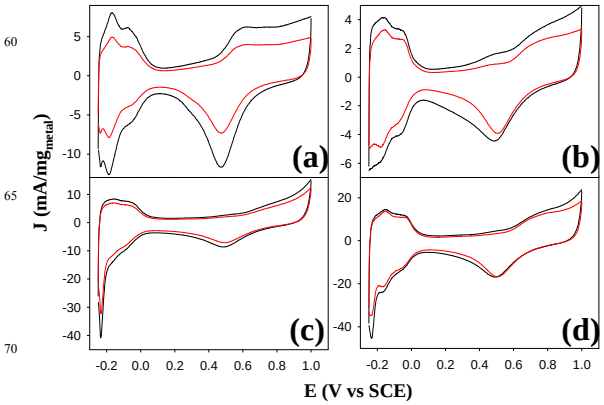

Fig. 5 The 1st (black curves) and 1000th (red curves) CV curves obtained on (a) commercial Pt/C, (b) PtPd/C, (c) PtPd/RGO, and (d) C-PtPd/RGO in 0.5 M H_2SO_4. Potential scan rate of 50 mV s^{-1}.

From the CVs of methanol oxidation on the different catalysts (Fig. 4b), the onset potential increases in the order of C-PtPd/RGO < PtPd/RGO < PtPd/C < Pt/C, indicating the highest activity of C-PtPd/RGO among the studied catalysts. Furthermore, the peak current density of MOR on C-PtPd/RGO is 381 mA mg^{-1}, which is nearly 2.24, 4.05, and 3.66 times larger than those on PtPd/RGO (170 mA mg^{-1}), PtPd/C (94 mA mg^{-1}) and commercial Pt/C catalysts (104 mA mg^{-1}), respectively. The long-term stability is another important criterion to evaluate the catalytic performance of a catalyst. Chronoamperometric (CA)

measurements at 0.60 V were then performed to study the catalytic stabilities of the electrocatalysts. As can be seen from Fig. 4c, after 1000s, the current density from the C-PtPd/RGO is higher (45.36 mA mg^{-1}) by a factor of 1.50, 2.09, and 1.51 than those obtained from the PtPd/RGO (30.3 mA mg^{-1}), Pt/C (21.72 mA mg^{-1}), and PtPd/C (30.03 mA mg^{-1}), demonstrating the highest electrocatalytic durability of the C-PtPd/RGO among the investigated catalysts. Fig. 4d compares the mass specific activities of the different electrocatalysts at 0.60 V. One can see that the C-PtPd/RGO shows the highest activity for methanol oxidation among the investigated catalysts.

To further examine the stability of the electrocatalysts, accelerated durability tests (ADTs) were also performed in 0.5 M H_2SO_4 + 0.5 M CH_3OH by applying a cyclic potential sweep between -0.25 and 1.0 V at a scan rate of 100 mV s^{-1}. The durability was then evaluated by comparing the ECSA of the catalysts and the peak currents of MOR before and after the accelerated methanol oxidation. As shown in Fig. 5 and Fig. S5, the C-PtPd/RGO lost only 9.96 % of the initial ECSA and nearly no loss of their forward peak current density after 1000 cycles. However, the degradation of commercial Pt/C, PtPd/C, and PtPd/RGO was quite severe, with 36.9%, 23.9%, and 18% of their initial ECSA and 23.1%, 12.1%, and 6.4% of their peak current density, respectively. These results further indicate that C-PtPd/RGO composites have enhanced durability toward methanol oxidation. From the present study, one can see that the graphene sheets-supported concave PtPd nanocrystals exhibit significantly enhanced catalytic performance for MOR and are less subject to dissolution, Ostawald ripening, and aggregation, compared to the convex-structured nanocrystals supported on carbon black. The excellent catalytic properties of C-PtPd/RGO could be ascribed to the specific concave structure with exposed high-index facets and the *in situ* growth of nanocrystals on graphene which could maximize the contact between nanocrystals and RGO, and thus enhance their interaction.

3. Conclusions

In the present report, for the first time, we demonstrated that PtPd concave alloy nanocubes enclosed by high-index {730} facets can be effectively tailored by GO nanosheets. Compared with the PtPd alloy nanocubes formed in the absence of GO, the concave nanocrystals exhibited much different size, shape, and composition, indicating the influence of GO on the initial nucleation and/or growth process of PtPd nanocrystals. Based on the TEM, XRD, and XPS analyses, the possible formation mechanism of C-PtPd/RGO was proposed, where small Pd nanoclusters were first formed on the RGO sheets and Pt component then grew gradually with reaction time. The as-prepared C-PtPd/RGO composites exhibited enhanced electrocatalytic activity and high durability in the methanol oxidation reaction compared with other investigated catalysts. The excellent catalytic performance could be attributed to the unique concave structure and strong interaction between PtPd nanocrystals and RGO sheets.

4. Experimental Section

4.1 Chemicals

Potassium tetrachloroplatinate (II) (K_2PtCl_4, 98%), sodium tetrachloropalladate (II) trihydrate (Na_2PdCl_4 • $3H_2O$, 99%), sodium iodide dehydrate (NaI•$2H_2O$, A.R., ≥99.0%), poly(vinyl pyrrolidone) (PVP, MW≈55000) were all obtained from Sigma-Aldrich. N, N-dimethylformamide (DMF, A. R., ≥99.5%), sulfuric acid (H_2SO_4, A.R., 95-98%), methanol (CH_3OH, A. R., ≥99.5%) were purchased from Beijing Chemical Works. The water used in all experiments was supplied by a Water Purifier Nanopure water system (18.3 M cm). All the chemicals were used as received without further purification. Moreover, all glasswares and Teflon-line were cleaned with Aqua Regia (HCl : HNO_3 with volume ratio of 3:1), followed by copious rinsing with ethanol and purified water. (Caution: Aqua Regia is a very corrosive oxidizing agent, which should be handled with great care.)

4.2 Synthesis of graphene supported PtPd concave nanocubes (C-PtPd/RGO)

Graphene oxide was synthesized from natural graphite by a modified Hummers method.[25, 29] In a typical synthesis of graphene supported PtPd concave nanocrystals, sodium tetrachloropalladate (Na_2PdCl_4, 20 mM, 1 mL), potassium tetrachloroplatinate (K_2PtCl4, 20 mM, 1 mL), sodium iodide (NaI•$2H_2O$, 100 mg) and poly(vinylpyrrolidone) (PVP, 170.0 mg) were mixed together with 10 mL DMF solution of GO in a 25.0-mL vial. After the vial was capped, the mixture was ultrasonicated for around 15 min. The resulting homogeneous mixture was then transferred into a conventional oven and heated at 130 °C for 5 h before it was cooled to room temperature. The resulting black colloidal products were precipitated by acetone, separated using a centrifugation, and further washed several times with an ethanol-acetone mixture. Finally, the obtained PtPd concave alloy nanocubes supported on RGO (C-PtPd/RGO) was dispersed in water for further use. It should be pointed out that the reaction time is one of the key parameters to determine the size and shape of the PtPd nanocrystals, as shown in Fig. 3. The final products obtained at other different temperatures (100, 150 and 180 °C) show the similar shape to that obtained at 130 °C.

4.3 Synthesis of carbon-supported PtPd alloy nanocubes (PtPd/C)

Unsupported PtPd alloy nanocubes were synthesized according to the reported procedure with some modification.[3] Carbon black (Vulcan XC-72) was then used as catalyst support to prepare PtPd alloy nanocubes catalyst (PtPd/C). In a typical preparation, carbon black was dispersed in water under sonication for 1 h. A certain amount of the as-prepared PtPd alloy nanocubes were then added into this dispersion at the nanoparticle/carbon black mass ratio of 20:80. This mixture was further sonicated for 30 min and stirred overnight. The resultant solids were precipitated by centrifugation and dried under a stream of nitrogen.

4.4 Synthesis of RGO-supported PtPd alloy nanocubes (PtPd/RGO)

RGO was synthesized according to the reported literatures.[17, 32, 33] In a typical synthesis, the DMF dispersion of GO (0.5 mg mL^{-1}) was heated to refluxing (~ 153 °C) for 4 h and cooled down to room temperature to convert GO to RGO. The synthesis process of RGO-supported PtPd alloy nanocubes is similar to that for

PtPd/C, except the use of RGO instead of carbon black.

4.5 Material Characterization

The size and shape of the as-synthesized materials were examined by using a Hitachi H-600 transmission electron microscope (TEM) operated at 100 kV. The samples were prepared by dropping a water dispersion of samples onto carbon-coated copper TEM grids using pipettes and dried under ambient condition. To examine the crystallinity of the products, power X-ray diffraction (XRD) was performed on a D8 ADVANCE (Germany) using Cu Kα radiation with a Ni filter (λ = 0.154059 nm at 30 kV and 15 mA). High-resolution TEM (HRTEM) images and EDX were both carried out on a JEM-2010 (HR) microscope operated at 200 kV. The compositions of the products were determined by an inductively coupled plasma-atomic emission spectrometer (ICP-AES, X Series 2, Thermo Scientific USA). X-ray photoelectron spectroscopy (XPS) measurements were performed by using a VG Thermo ESCALAB 250 spectrometer (VG Scientific) operated at 120 W. The binding energy was calibrated against the carbon 1s line.

4.6 Electrochemical measurements

Before each experiment, a glassy carbon (GC) electrode (5.62 mm in diameter) was first polished with alumina slurries (Al_2O_3, 0.05 μm) on a polishing cloth to obtain a mirror finish, followed by sonication in ethanol and pure water for 10 min, successively. To prepare a catalyst-coated working electrode, catalyst was dispersed in a mixture of solvents containing water, isopropanol and Nafion (5%) (v/v/v = 4/1/0.025) to form a 1 mg mL^{-1} suspension. A calculated amount of the catalyst ink was then dropcast onto the polished GC electrode and dried at room temperature under a gentle flow of nitrogen.

Voltammetric measurements were carried out with a CHI 750D electrochemical workstation. The electrode prepared above was used as the working electrode. A saturated calomel electrode (SCE) combination isolated in a double junction chamber and a Pt coil was used as the reference and counter electrodes, respectively. All electrode potentials in the present study were referred to this SCE reference. The working electrodes were first activated with cyclic voltammograms (CVs) (-0.25 to 1.0 V at 100 mV s^{-1}) in N_2-purged 0.5 M H_2SO_4 solution until a steady CV was obtained. To measure the methanol electro-oxidation, a solution of 0.5 M H_2SO_4 + 0.5 M CH_3OH was purged with N_2 gas before measurements were taken, and the CVs were recorded in a potential window between -0.25 and 1.0 V at a scan rate of 50 mV s-1. The amperometric current density-time (i-t) curves were measured at a fixed potential of 0.60 V for 1000 s in 0.5 M H_2SO_4 + 0.5 M CH_3OH. For each catalyst, the current was normalized to the loading of noble metals (Pt + Pd) to obtain mass activity. All experiments were conducted at room temperature.

Acknowledgements

This work was supported by the National Natural Science Foundation of China (No. 21275136) and the Natural Science Foundation of Jilin province, China (No. 201215090).

Notes and references

[a] *State Key Laboratory of Electroanalytical Chemistry, Changchun Institute of Applied Chemistry, Chinese Academy of Sciences, Changchun 130022, Jilin, China. Tel: +86431-85262061; E-mail: weichen@ciac.ac.cn*

[b] *University of Chinese Academy of Sciences, Beijing 100039, China*

† Electronic Supplementary Information (ESI) available: Additional structural characterizations and electrochemical measurements. See DOI: 10.1039/b000000x/

1. H. J. Lee, S. E. Habas, G. A. Somorjai and P. D. Yang, J. Am. Chem. Soc., 2008, 130, 5406-5407.
2. B. Lim, M. J. Jiang, P. H. C. Camargo, E. C. Cho, J. Tao, X. M. Lu, Y. M. Zhu and Y. N. Xia, Science, 2009, 324, 1302-1305.
3. X. Q. Huang, Y. J. Li, Y. J. Li, H. L. Zhou, X. F. Duan and Y. Huang, Nano Lett., 2012, 12, 4265-4270.
4. S. E. Habas, H. Lee, V. Radmilovic, G. A. Somorjai and P. Yang, Nat. Mater., 2007, 6, 692-697.
5. J. Zhang, K. Sasaki, E. Sutter and R. R. Adzic, Science, 2007, 315, 220-222.
6. V. R. Stamenkovic, B. Fowler, B. S. Mun, G. F. Wang, P. N. Ross, C. A. Lucas and N. M. Markovic, Science, 2007, 315, 493-497.
7. R. Narayanan and M. A. El-Sayed, Nano Lett., 2004, 4, 1343-1348.
8. C. Wang, H. Daimon, T. Onodera, T. Koda and S. H. Sun, Angew. Chem. Int. Edit., 2008, 47, 3588-3591.
9. J. Zhang and J. Y. Fang, J. Am. Chem. Soc., 2009, 131, 18543-18547.
10. N. Tian, Z. Y. Zhou, S. G. Sun, Y. Ding and Z. L. Wang, Science, 2007, 316, 732-735.
11. Z. Y. Zhou, Z. Z. Huang, D. J. Chen, Q. Wang, N. Tian and S. G. Sun, Angew. Chem. Int. Edit., 2010, 49, 411-414.
12. X. Q. Huang, Z. P. Zhao, J. M. Fan, Y. M. Tan and N. F. Zheng, J. Am. Chem. Soc., 2011, 133, 4718-4721.
13. L. Zhang, J. W. Zhang, Q. Kuang, S. F. Xie, Z. Y. Jiang, Z. X. Xie and L. S. Zheng, J. Am. Chem. Soc., 2011, 133, 17114-17117.
14. J. A. Zhang, M. R. Langille, M. L. Personick, K. Zhang, S. Y. Li and C. A. Mirkin, J. Am. Chem. Soc., 2010, 132, 14012-14014.
15. M. S. Jin, H. Zhang, Z. X. Xie and Y. N. Xia, Angew. Chem. Int. Edit., 2011, 50, 7850-7854.
16. C. J. DeSantis, A. A. Peverly, D. G. Peters and S. E. Skrabalak, Nano Lett., 2011, 11, 2164-2168.
17. C. D. Donega, Chem. Soc. Rev., 2011, 40, 1512-1546.
18. Y. J. Li, Y. J. Li, E. B. Zhu, T. McLouth, C. Y. Chiu, X. Q. Huang and Y. Huang, J. Am. Chem. Soc., 2012, 134, 12326-12329.
19. X. M. Ma, H. Meng, M. Cai and P. K. Shen, J. Am. Chem. Soc., 2012, 134, 1954-1957.
20. S. H. Sun, G. X. Zhang, D. S. Geng, Y. G. Chen, R. Y. Li, M. Cai and X. L. Sun, Angew. Chem. Int. Edit., 2011, 50, 422-426.
21. M. Jahan, Q. L. Bao and K. P. Loh, J. Am. Chem. Soc., 2012, 134, 6707-6713.
22. Y. Y. Jiang, Y. Z. Lu, X. Y. Lv, D. X. Han, Q. X. Zhang, L. Niu and W. Chen, Acs Catal., 2013, 3, 1263-1271.
23. S. J. Guo and S. H. Sun, J. Am. Chem. Soc., 2012, 134, 2492-2495.
24. M. S. Zhu, P. L. Chen and M. H. Liu, Langmuir, 2013, 29, 9259-9268.
25. Y. Z. Lu, Y. Y. Jiang, H. B. Wu and W. Chen, J. Phys. Chem. C., 2013, 117, 2926-2938.
26. D. Y. Sung, J. L. Gunjakar, T. W. Kim, I. Y. Kim, Y. R. Lee and S. J. Hwang, Chem.-Eur. J., 2013, 19, 7109-7117.
27. X. Q. Huang, H. H. Zhang, C. Y. Guo, Z. Y. Zhou and N. F. Zheng, Angew. Chem. Int. Edit., 2009, 48, 4808-4812.
28. R. F. Nie, J. H. Wang, L. N. Wang, Y. Qin, P. Chen and Z. Y. Hou, Carbon, 2012, 50, 586-596.
29. Y. Z. Lu, Y. Y. Jiang, W. T. Wei, H. B. Wu, M. M. Liu, L. Niu and W. Chen, J. Mater. Chem., 2012, 22, 2929-2934.
30. Y. Z. Lu, Y. Y. Jiang, R. Z. Zhang and W. Chen, Sci. Adv. Mater., 2013, 5, 1718-1726.
31. Y. Z. Lu, Y. Y. Jiang and W. Chen, Nano Energy, 2013, 2, 836-844.
32. D. Xu, S. Bliznakov, Z. P. Liu, J. Y. Fang and N. Dimitrov, Angew. Chem. Int. Edit., 2010, 49, 1282-1285.
33. K. L. Ai, Y. L. Liu, L. H. Lu, X. L. Cheng and L. H. Huo, J. Mater. Chem., 2011, 21, 3365-3370.